Coverage in Millimeter-Wave Networks with SNR-Dependent Beam Alignment Errors

Muhammad Saad Zia, Douglas M. Blough and Mary Ann Weitnauer
School of Electrical and Computer Engineering
Georgia Institute of Technology, Atlanta, Georgia 30332-0250, USA
Email: saad.zia@gatech.edu; doug.blough@ece.gatech.edu; mary.ann.weitnauer@ece.gatech.edu

***Abstract*—Narrow beamwidth and inaccurate angle-of-arrival (AoA) estimation make perfect beam alignment difficult in millimeter-wave (mm-wave) systems. The extent of beam misalignment depends on the uplink received signal-to-noise ratio (SNR) at a single antenna element of the array. Using stochastic geometry, this paper analyzes and quantifies the loss in downlink SNR coverage probability due to beam misalignment. The standard deviation of the beam alignment error is obtained through the Cramér-Rao lower bound (CRLB) of AoA estimation. The analytical results are verified through Monte-Carlo simulations and it is shown that the beam alignment errors affect the system coverage significantly when the downlink SNR threshold (with array gain) is less than 5 dB. It is also illustrated that increasing the number of antennas alone cannot counter the effects of beam alignment errors.**

***Index Terms*—Millimeter-wave, beam alignment error, beamwidth, antenna radiation pattern, Cramér-Rao lower bound.**

I. Introduction

The millimeter-wave (mm-wave) frequencies (28–300 GHz) offer enormous bandwidth and are thus lucrative for 5G and beyond [1], [2]. A key differentiating feature of mm-wave frequencies is the sensitivity to blockages and high path loss. Thus, highly directional transmissions are required to achieve satisfactory performance at mm-wave frequencies.

The maximum array gain is achieved by steering the main beam in the desired direction using beam alignment algorithms based on the angle-of-arrival (AoA) estimation [3]. In practice, the beam alignment algorithms introduce some error resulting in a suboptimal array gain [2], [4]. It is, therefore, important to analyze the effect of beam misalignment on the performance of mm-wave networks.

In [5], the authors investigate the effects of beam misalignment on the throughput and coverage of an *ad-hoc* wireless network using tools from stochastic geometry but do not incorporate the propagation characteristics of mm-wave communications. The loss in ergodic capacity of a mm-wave *ad-hoc* network has been characterized in [3] using the sectored and the Gaussian antenna models and it is shown that the sectored or "flat-top" antenna model is not suitable for studying the effects of beam alignment errors. The works in [2] and [4] provide a comprehensive analysis of beam misalignment but do not consider the dependence of beam alignment errors on the quality of AoA estimation.

This paper uses the Cramér-Rao lower bound (CRLB) of AoA estimates to obtain the variance of the beam alignment error. Specifically, the actual antenna array pattern is approximated by a simpler radiation pattern that captures the effects of beam alignment errors more accurately than the sectored antenna model. The distribution of the uplink received signal-to-noise ratio (SNR) at a single antenna element is derived and the variance of the beam alignment error is approximated thereof using the expression of CRLB. The truncated Gaussian distribution is utilized to characterize the beam alignment errors and the performance of the network is analyzed in terms of the downlink SNR coverage probability. This is motivated by the fact that mm-wave systems are noise limited and the throughput of a network depends on the SNR [6]. A comparison of the coverage probabilities obtained through perfect and imperfect beam alignment illustrates that the performance of mm-wave networks is not solely dependent on the number of antennas per base station.

II. System Model

This paper considers the downlink of a mm-wave cellular network where all the BSs are distributed in $\mathbb{R}^2$ according to a homogeneous Poisson point process Φ_{B} with intensity measure λ_{B}. The BSs transmit at a constant power P_{d}. As per the Slivnyak's theorem, the analysis in this paper is conducted for a *typical user* placed at the origin, $\mathcal{O}$ [1], [7], [8].

The blockage effects are modeled using the modified line-of-sight (LOS) ball model in which the LOS region around each transmitter/ receiver is approximated as a ball of fixed radius R_{B} [6]. Inside the ball, mm-wave links can be categorized into LOS and non-line-of-sight (NLOS) links and the value of R_{B} represents the range of a LOS link. The probability of a mm-wave link with length r being LOS is given in [8] as $\mathcal{P}_{\mathrm{L}}(r) = \mu \cdot \mathbb{1}(r < R_{\mathrm{B}})$, where μ is the average fraction of the LOS area inside the ball and $\mathbb{1}(\cdot)$ is the indicator function.

Blockage induces different path-loss for LOS and NLOS channel states. The path-loss between the typical UE and the serving BS, with channel state k and located at x, is represented as $L_k(x) = C_k \|x\|^{-\alpha_k}$ where C_k and α_k are the path-loss intercept and path-loss exponent of the channel state k, respectively, and $k \in \{L, N\}$. For brevity, the LOS and NLOS channel states are denoted as "L" and "N" respectively in the rest of this paper. The UE is served by the BS that offers the minimum path loss i.e., the maximum average received power. A single omnidirectional antenna is assumed at the UE.

978-1-7281-5207-3/20/$31.00 ©2020 IEEE

TABLE I
NOTATION AND DEFAULT SYSTEM PARAMETERS

Notation	Description	Value
λ_{B}	BS density	$50/\mathrm{km}^2$
P_{d}	Downlink transmit power	30 dBm
P_{u}	Uplink transmit power	23 dBm
f_{c}	Carrier frequency	28 GHz
W	Bandwidth	1 GHz
$\alpha_{\mathrm{L}}, \alpha_{\mathrm{N}}$	LOS and NLOS path loss exponents respectively	2, 2.92
$C_{\mathrm{L}}, C_{\mathrm{N}}$	LOS and NLOS path loss intercepts respectively	-61.4 dB, -72 dB
$N_{\mathrm{L}}, N_{\mathrm{N}}$	Nakagami shape parameters for LOS and NLOS signals	3, 2
σ_n^2	Noise power	-174 dBm/Hz $+ 10\log_{10}(W) + 10$ dB
μ, R_{B}	LOS ball model parameters	0.2, 200 m

Antenna arrays composed of directional antenna elements are assumed at the BS to provide high directivity gains. The power radiated by a single antenna element in a direction ϕ is specified by the antenna element pattern $G_e(\phi)$. Mathematically, the element radiation pattern is defined as [5]

$$G_e(\phi) = \begin{cases} G_{\max} 10^{\frac{-3}{10}\left(\frac{2\phi}{\varphi_e}\right)^2} & \text{if } |\phi| \leq \Theta_e \\ G_{\mathrm{s}} & \text{if } \Theta_e \leq |\phi| \leq \pi, \end{cases} \quad (1)$$

where $G_{\max}$ is the maximum directional gain of the single element which is obtained at the boresight, G_{s} is the average sidelobe gain, φ_e is the half-power beamwidth (HPBW) and Θ_e is the mainlobe beamwidth given by $\Theta_e = (\varphi_e/2)\sqrt{(10/3)\log_{10}(G_{\max}/G_{\mathrm{s}})}$. As per the 3GPP specifications adopted in [10], $G_{\max} = 8$ dBi, $G_{\mathrm{s}} = -22$ dBi, $\varphi_e = 65°$ and $\Theta_e = 102.8°$. Moreover, each BS utilizes three sectors to provide coverage. The field of view of a sector is, therefore, $\left[-\frac{\pi}{3}, \frac{\pi}{3}\right]$. Each sector is equipped with a uniform linear array (ULA) comprising M directional antenna elements. The array response pattern, $G_{\mathrm{A}}(\phi, \theta)$, is obtained by

$$G_{\mathrm{A}}(\phi, \theta) = G_{\mathrm{e}}(\phi) \cdot \mathrm{AF}(\phi, \theta), \quad (2)$$

where $\phi \in \left[\frac{-\pi}{3}, \frac{\pi}{3}\right]$ is the AoA, $\theta \in \left[\frac{-\pi}{3}, \frac{\pi}{3}\right]$ represents the mainlobe steering direction and $\mathrm{AF}(\phi, \theta)$ is the array factor which depends on the number of antenna elements and the physical array configuration. The subscripts e and A stand for the single element and array respectively. The array factor is represented as $\mathrm{AF}(\phi, \theta) = |\mathbf{a} \cdot \mathbf{w}|^2$, where $\mathbf{a} \in \mathbb{C}^M$ is the vector of beamforming weights and $\mathbf{w} \in \mathbb{C}^M$ is the channel response vector, which depends on the angle ϕ. For a ULA, the channel response vector is given by

$$\mathbf{w}(\phi) = \left[1, e^{\frac{j2\pi d}{\lambda_c}\sin(\phi)} \cdots, e^{\frac{j2\pi(M-1)d}{\lambda_c}\sin(\phi)}\right], \quad (3)$$

where d is the spacing between adjacent antenna elements which is kept at half-wavelength and λ_c is the carrier wavelength. The beamforming vector $\mathbf{a}(\theta)$ is the same as $\mathbf{w}(\phi)$ but scaled by $1/\sqrt{M}$ and with ϕ replaced by θ.

Small-scale fading is assumed to be independent for each link and modeled using the Nakagami distribution. With Nakagami fading, the received power is gamma distributed. Different Nakagami shape parameters, N_{L} and N_{N}, are assumed for LOS and NLOS propagation respectively. For analytical tractability, N_{L} and N_{N} are assumed to be integers [2], [7].

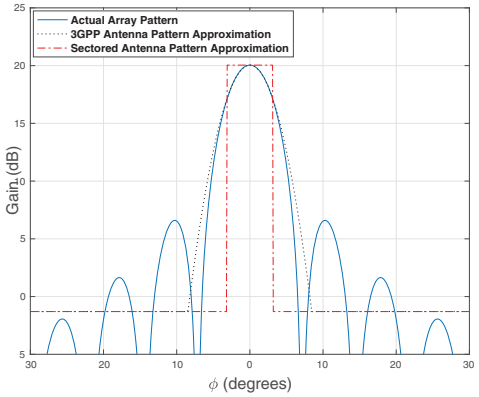

Fig. 1. Antenna array radiation pattern with 16 elements and $\theta = 0°$

Analyzing the performance of the network with the actual array radiation pattern using (2) is not feasible [10]. Therefore, the actual array radiation pattern is approximated using the 3GPP antenna model in (1) as done in [11]. The broadside HPBW, φ_A, of the ULA is computed as [12]

$$\varphi_A = \pi - 2\cos^{-1}\left(\frac{1.391}{\pi M d}\right). \quad (4)$$

The peak mainlobe gain, G_1, and the average sidelobe gain, G_2, of the ULA are computed as in [10]

$$G_1(\phi) = G_e(\phi)\ M, \qquad G_2 = \frac{1}{M\sin^2\left(\frac{3\pi}{2M}\right)}. \quad (5)$$

Using (4)–(5), the approximated array radiation pattern, $\widetilde{G}_A(\phi, \theta)$ can be written as

$$\widetilde{G}_A(\phi, \theta) = \begin{cases} G_1(\phi)\, 10^{\frac{-3}{10}\left(\frac{2(\phi-\theta)}{\varphi_A}\right)^2} & \text{if } |\phi - \theta| \leq \Theta_A \\ G_2 & \text{if } \Theta_A \leq |\phi - \theta| \leq \pi, \end{cases} \quad (6)$$

where $\Theta_A = (\varphi_A/2)\sqrt{(10/3)\log_{10}[G_1(\phi)/G_2]}$ is the main lobe beamwidth of the approximated array radiation pattern corresponding to a specific value of true AoA ϕ. We define the beam alignment error to be $\epsilon = (\phi - \theta)$. Since $\widetilde{G}_A(\phi, \theta)$ depends on $(\phi - \theta)$ and ϕ itself, we express the array response as $\widetilde{G}_A(\phi, \epsilon)$ in the remainder of this paper.

Fig. 1 illustrates the relation between the proposed approximated array radiation pattern and the actual array radiation pattern for $\theta = 0°$. The sectored antenna model widely used in the existing literature (e.g., [2], [7]), is also shown for comparison. As compared to the sectored antenna model, the proposed approximation better models the main lobe gain. In fact, the approximated pattern exactly matches the actual pattern up till the HPBW making it a good fit to study the effects of beam alignment errors in directional mm-wave cellular networks.

The beam alignment error, ϵ, is assumed to follow a truncated-Gaussian distribution with zero mean [2], [3]. Moreover, the absolute value of the error is bounded by the main lobe beamwidth [11], i.e., $|\epsilon| \leq \Theta_A$. This is because an error

exceeding the main lobe beamwidth is merely an alignment failure and no transmission occurs under such a scenario. The probability density function (PDF) of a truncated Gaussian distribution is given as

$$f_{\epsilon}(t) = \frac{\sqrt{\frac{2}{\pi\sigma_{\epsilon}^2}}\exp\left(\frac{-t^2}{2\sigma_{\epsilon}^2}\right)}{\operatorname{erf}\left(\frac{\Theta_A}{\sqrt{2}\sigma_{\epsilon}}\right) - \operatorname{erf}\left(\frac{-\Theta_A}{\sqrt{2}\sigma_{\epsilon}}\right)}, \qquad t \in [-\Theta_A, \Theta_A] \quad (7)$$

where $\operatorname{erf}(\cdot)$ is the error function and σ_{ϵ} is the standard deviation of the beam alignment error. In prior works (e.g., [2], [4]), σ_{ϵ} was chosen arbitrarily to generate a specific mean absolute error. However, in practical beam alignment algorithms, the value of σ_{ϵ} is dependent on the AoA estimation. In this paper, σ_{ϵ} is obtained from the CRLB of AoA estimation. The CRLB is a theoretical bound which gives the lowest estimation variance of any unbiased estimator. The CRLB of the AoA estimate is obtained by inverting the Fischer Information (FI) [13]. For channel state k, it can be expressed as

$$CRLB \triangleq \sigma_{\epsilon_k}^2 = \Delta_k^{-1}, \quad (8)$$

where Δ_k is the FI corresponding to the AoA estimate. From [9] and [13], the expression of Δ_k for a ULA can be written as a function of two parameters and is given as

$$\Delta_k(\phi, \gamma_k) = \left(\frac{2\pi f_c d\cos(\phi)}{c}\right)^2 \frac{M\left(M^2-1\right)\gamma_k}{6}, \quad (9)$$

where f_c is the carrier frequency, c is the speed of light, ϕ is the true AoA and γ_k is the uplink received SNR at a single BS antenna element.

III. Uplink Received SNR Distribution for a Single Antenna Element

Because the downlink steering error depends on the uplink SNR received at a single antenna element, the uplink SNR distribution is derived in this section. If the typical UE is served by a BS with channel state k, then the uplink received SNR, γ_k, at a single directional antenna element of the BS sector can be formulated as

$$\gamma_k = \frac{P_{\mathrm{u}} G_e(\phi)\, \varrho_x L_k(x)}{\sigma_n^2}, \quad (10)$$

where P_{u} is the uplink transmit power, ϱ_x is the channel gain due to small-scale fading on the link and σ_n^2 is the noise power. The CDF of γ_k is expressed as

$$\begin{aligned}
\tilde{\mathcal{F}}_{\gamma_k}(\tau) &= \mathbb{P}(\gamma_k \le \tau | k) \\
&\overset{(a)}{=} \mathbb{P}\left(\varrho_x \le \frac{\tau\sigma_n^2}{P_{\mathrm{u}}\, G_e(\phi)\, L_k(x)} \;\middle|\; k\right) \\
&\overset{(b)}{\approx} \mathbb{E}_{x,\phi}\left(\left[1 - \exp\left(\frac{-\beta_k \tau\sigma_n^2}{P_{\mathrm{u}}\, G_e(\phi)\, L_k(x)}\right)\right]^{N_k} \;\middle|\; k\right) \\
&\overset{(c)}{=} 1 + \sum_{n=1}^{N_k} (-1)^n \binom{N_k}{n} \\
&\quad \times \int_{x=0}^{\infty}\int_{\phi} e^{\left(\frac{-\beta_k n\tau\sigma_n^2}{P_{\mathrm{u}} G_e(\phi) L_k(x)}\right)} f_{\phi}(\phi)\, \hat{f}_k(x)\, \mathrm{d}\phi\, \mathrm{d}x,
\end{aligned} \quad (11)$$

where $\beta_k = N_k (N_k!)^{\frac{-1}{N_k}}$, $\hat{f}_k(x)$ is the PDF of the distance to the serving BS [7], [8], (a) follows directly from (10), (b) is obtained from the CDF approximation of the gamma random variable [7] and (c) is obtained by applying the binomial theorem and the expectation operator on (b).

The field of view of each BS sector is $\left[-\frac{\pi}{3}, \frac{\pi}{3}\right]$, hence, ϕ is assumed to be distributed uniformly within this interval with $f_{\phi}(\phi) = \frac{3}{2\pi}$. The value of $\hat{f}_k(x)$ is given in [7] and [8] as

$$\hat{f}_k(x) = \frac{f_k(x)}{\mathcal{A}_k} \exp\left(-2\pi\lambda_{\mathrm{B}} \int_0^{\chi_k(x)} t\left(1 - \mathcal{P}_k(t)\right) \mathrm{d}t\right), \quad (12)$$

where $\chi_{\mathrm{L}}(x) = (C_{\mathrm{N}}/C_{\mathrm{L}})^{1/\alpha_{\mathrm{N}}} (x)^{\alpha_{\mathrm{L}}/\alpha_{\mathrm{N}}}$, $\chi_{\mathrm{N}}(x) = (C_{\mathrm{L}}/C_{\mathrm{N}})^{1/\alpha_{\mathrm{L}}} (x)^{\alpha_{\mathrm{N}}/\alpha_{\mathrm{L}}}$ and $f_k(x)$ is the PDF of distance of typical UE from its nearest BS with channel state k given as

$$f_k(x) = 2\pi\lambda_{\mathrm{B}}\; x\mathcal{P}_k(x) \exp\left(-2\pi\lambda_{\mathrm{B}} \int_0^x x\mathcal{P}_k(x)\, \mathrm{d}x\right), \quad (13)$$

The term $\mathcal{A}_k$ represents the probability of the typical UE being associated with a BS with channel state k and is given as [8]

$$\mathcal{A}_k = \int_0^{\infty} f_k(x) \exp\left(-2\pi\lambda_{\mathrm{B}} \int_0^{\chi_k(x)} t\left(1 - \mathcal{P}_k(t)\right) \mathrm{d}t\right) \mathrm{d}x. \quad (14)$$

The PDF, f_{γ_k}, of the SNR γ_k is obtained by differentiating (11) with respect to τ

$$\begin{aligned}
f_{\gamma_k}(\tau) = \tau \frac{\ln(10)}{10} \sum_{n=1}^{N_k} (-1)^n \binom{N_k}{n} \\
\times \int_0^{\infty}\int_{\phi} \frac{-\beta_k n\sigma_n^2}{P_{\mathrm{u}} G_{\mathrm{e}}(\phi) L_k(x)} \cdot e^{\left(\frac{-\beta_k n\tau\sigma_n^2}{P_{\mathrm{u}} G_{\mathrm{e}}(\phi) L_k(x)}\right)} \\
\times f_{\phi}(\phi)\, \hat{f}_k(x)\, \mathrm{d}\phi\, \mathrm{d}x.
\end{aligned} \quad (15)$$

Using the law of total probability, the total UL SNR at a single BS antenna is obtained as $f_{\gamma}(\tau) = \sum_k \mathcal{A}_k f_{\gamma_k}(\tau)$. The integrand in (15) is the joint PDF of γ_k, ϕ and x. It follows that integrating this integrand only over x yields the joint PDF of γ_k and ϕ which is represented by $f_{(\phi,\gamma_k)}(\phi, \tau)$.

IV. Beam Alignment Error and Downlink SNR Coverage Analysis

The SNR coverage probability, $\mathcal{C}(\tau)$, is defined as the probability that the *downlink* received SNR, Ω, is greater than a certain threshold τ, i.e., $\mathcal{C}(\tau) = \mathbb{P}(\Omega > \tau)$. The conditional SNR coverage probability, $\mathcal{C}_k(\tau)$, conditioned on channel state k, is expressed as

$$\mathcal{C}_k(\tau) = \mathbb{P}(\Omega_k > \tau) \triangleq \mathbb{P}\left(\frac{P_{\mathrm{d}}\, \widetilde{G}_A(\phi, \epsilon)\, \varrho_x L_k(x)}{\sigma_n^2} > \tau \;\middle|\; k\right). \quad (16)$$

The associated BS determines the AoA based on the uplink received SNR from the typical UE and steers the beam towards the desired direction. With perfect beam alignment, the array gain equals the maximum gain, $G_1(\phi)$, corresponding to a

specific value of ϕ. However, perfect beam alignment is hard to realize due to errors in AoA estimation. To simplify the analysis and to enable us to use the approach of [2], we average out the dependence of CRLB on ϕ. At a certain value of uplink SNR, the variance of the beam alignment error for channel state k is approximated from (8) and (9) as

$$\sigma_{\epsilon}^{2}(\tau) \approx \left(\int_{\phi} \Delta_{k}(\phi,\tau)\, f_{(\phi,\gamma_k)}(\phi,\tau)\, \mathrm{d}\phi \right)^{-1}. \tag{17}$$

The accuracy of the above approximation is validated in Section V through Monte-Carlo simulations. With beam alignment errors, the array gain can be formulated as a RV given by the following lemma

Lemma 1. *If $f_{\epsilon_k}(t)$ is the statistical distribution of the beam alignment error, then the conditional PDF of array gain given a certain value of ϕ is expressed as*

$$f_{(\widetilde{G}_A|\phi)}(g|\phi) = 2 f_{\epsilon_k}\left(\sqrt{\frac{-5}{6}\log_{10}\left(\frac{g}{G_1(\phi)}\right)}\varphi_A \right) \times \frac{5}{12} \frac{\varphi_A}{\sqrt{\frac{-5}{6}\log_{10}\left(\frac{g}{G_1(\phi)}\right)}} \frac{1}{g\ln(10)} \tag{18}$$

where $g \in [G_2,\, G_1(\phi)]$.

Proof. Since the error is bounded by the mainlobe beamwidth, application of the method of transformation of RVs on (6) yields $\epsilon(g|\phi) = \varphi_A \sqrt{(-5/6)\log_{10}(g/G_1(\phi))}$. The PDF of a function of a RV is expressed as

$$f_{\widetilde{G}_A}(g|\phi) = f_{\epsilon}(\epsilon(g|\phi)) \cdot \left| \frac{\mathrm{d}}{\mathrm{d}g}\left[\epsilon(g|\phi)\right] \right|. \tag{19}$$

Plugging in the value of $\epsilon(g|\phi)$ in (19) completes the proof. The constant factor of 2 in (18) arises due to the symmetry of the array radiation pattern around the boresight. ■

Using the same procedure as in (11), $\mathcal{C}_k(\tau)$ is obtained as follows

$$\begin{aligned}
\mathcal{C}_k(\tau) &= \mathbb{P}\left(\varrho_x > \frac{\tau\sigma_n^2}{P_{\mathrm{d}}\, \widetilde{G}_A(\phi,\epsilon)\, L_k(x)} \,\middle|\, k \right) \\
&\overset{(a)}{\approx} 1 - \mathbb{E}_{x,\widetilde{G}_A}\left(\left[1 - e^{\left(\frac{-\beta_k \tau \sigma_n^2}{P_{\mathrm{d}} G_A(\phi,\epsilon) L_k(x)} \right)} \right]^{N_k} \,\middle|\, k \right) \\
&\overset{(b)}{=} -\sum_{n=1}^{N_k} (-1)^n \binom{N_k}{n} \\
&\times \int_0^{\infty} \int_{\phi} \int_{g} e^{\left(\frac{-\beta_k n \tau \sigma_n^2}{P_{\mathrm{d}} g L_k(x)} \right)} f_{\widetilde{G}_A}(g|\phi)\, \mathrm{d}g\; f_{\phi}(\phi)\, \mathrm{d}\phi \\
&\times \hat{f}_k(x)\, \mathrm{d}x,
\end{aligned} \tag{20}$$

where (a) follows from the CCDF approximation of the gamma random variable [7] and (b) follows by applying the binomial theorem and the definition of the expectation operator. The total downlink coverage probability can be expressed as $\mathcal{C}(\tau) = \sum_{k\in\{L,N\}} \mathcal{A}_k \mathcal{C}_k(\tau)$.

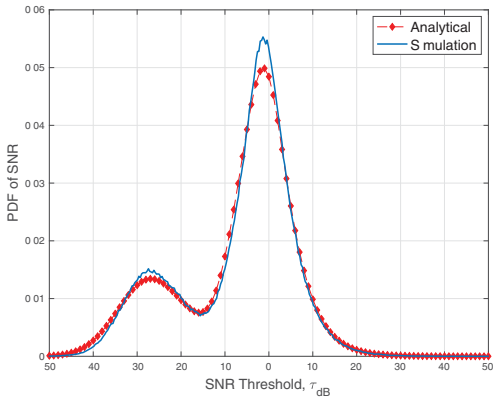

Fig. 2. PDF of uplink received SNR at a single antenna element of the BS.

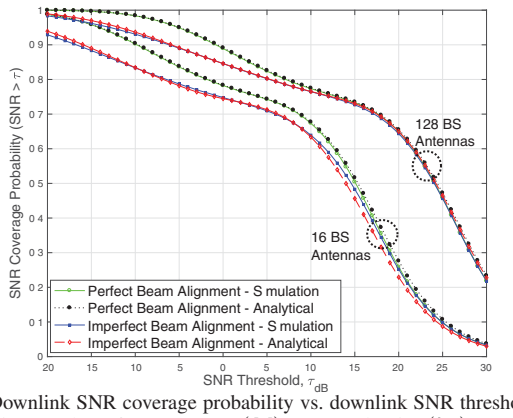

Fig. 3. Downlink SNR coverage probability vs. downlink SNR threshold (τ) with varying number of BS antennas (M) at a BS density $(\lambda_{\mathrm{B}}) = 50/\mathrm{km}^2$.

V. Numerical Results and Discussion

This section evaluates the performance of a mm-wave network in the presence of beam alignment errors and verifies the accuracy of the developed analytical framework through Monte-Carlo simulations. The simulation model is based on the exact expression of σ_{ϵ}^2 given in (8) and (9). Moreover, the actual gamma-distributed received power is incorporated in both the uplink and downlink directions. For each simulation, 10^6 trials are conducted. The default network parameters and notations are listed in Table 1 for convenience.

The PDF of the uplink received SNR at a single BS antenna element is illustrated in Fig. 2. The derived analytical results match very well with the simulation results. The big peak at around 0 dB is due to the LOS propagation and the small peak at around -30 dB is due to NLOS propagation. The discrepancy in the heights of these two peaks represents that majority of the communication in mm-wave networks takes place due to LOS signals.

Fig. 3 compares the downlink SNR coverage probabilities obtained from perfect beam alignment and imperfect beam alignment for two different numbers of BS antennas. The analytical curves match very well with the simulation results for all the cases, hence validating the analytical framework developed above. For perfect alignment, the coverage with $M = 128$ is simply a right shifted version of the coverage

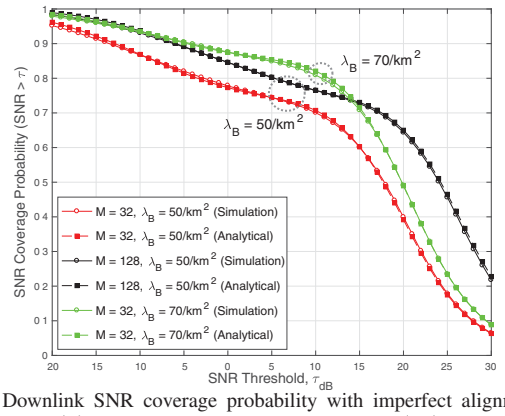

Fig. 4. Downlink SNR coverage probability with imperfect alignment vs. SNR threshold (τ) for varying number of BS antennas (M) and BS density (λ_{B}).

with $M = 16$. The amount of shift is equal to the difference between the array directivity gains for the two configurations i.e., 9 dB in this case. The same, however, is not true for the coverage probabilities with imperfect alignment.

For $\tau < 5$ dB, where systems using error correction codes are likely to operate, the difference between the perfect alignment coverage probability and imperfect alignment coverage probability is quite high for both antenna configurations. This difference tends to decrease as the system transitions towards a high SNR regime and almost vanishes at a certain SNR threshold. However, for $M = 128$, the difference vanishes at a comparatively lower SNR threshold value. For example, at coverage probability equal to 0.8, the difference in SNR threshold values for perfect and imperfect alignment is about 5 dB for $M = 16$. The same difference comes out to be 2 dB for $M = 128$. This is because the variance of beam alignment errors is inversely proportional to M^3 as shown in (8)–(9). While increasing M reduces the effects of beam alignment errors, the reduction is more pronounced for high SNR regime as compared to low SNR regime. Increasing M from 16 to 128 reduces the difference between perfect alignment coverage and imperfect alignment coverage by about 3 dB at a coverage probability of 0.7 but only by 1 dB at a coverage probability of 0.9. This is due to the dependence of beam alignment errors on the uplink received SNR at a single antenna element of the BS. The above discussion implies that the beam alignment errors degrade the performance of a mm-wave network significantly in low SNR regime as compared to high SNR regime; and increasing the number of antennas does not completely eliminate this degradation of performance.

The effect of increasing the BS density on the coverage probability with imperfect alignment is illustrated in Fig. 4. Two of the curves have the same $\lambda_{\mathrm{B}} = 50/\mathrm{km}^2$ and differ only in the value of M while one of the curves has $M = 32$ and $\lambda_{\mathrm{B}} = 70/\mathrm{km}^2$. At both these values of λ_{B}, the mm-wave systems are considered to be noise-limited [6]. With $M = 32$ antennas, the coverage probabilities for $\lambda_{\mathrm{B}} = 50/\mathrm{km}^2$ and $\lambda_{\mathrm{B}} = 70/\mathrm{km}^2$ begin to drop rapidly at about $\tau = 10$ dB. This sudden drop is due to the blockage caused by the LOS ball model. At $\tau = 10$ dB and $M = 32$, the coverage with $\lambda_{\mathrm{B}} = 50/\mathrm{km}^2$ is only about 71% while it is more than 82% with $\lambda_{\mathrm{B}} = 70/\mathrm{km}^2$. This illustrates that by increasing the λ_{B} from $50/\mathrm{km}^2$ to $70/\mathrm{km}^2$, an additional 11% of UEs are considered to be inside the LOS ball. If λ_{B} is kept fixed at $50/\mathrm{km}^2$ and M is increased from 32 to 128 at $\tau = 10$ dB, the coverage probability only increases by 5.8%. This shows that, while expensive, increasing the BS density with a lower number of antennas per BS is more effective than increasing the number of antennas per BS with a lower BS density, for -10 dB $\leq \tau \leq 14$ dB.

VI. Conclusion

This paper analyzes the impacts of SNR-dependent beam alignment errors on the downlink coverage probability of mm-wave networks. It is shown that the errors affect the coverage probability differently in high and low SNR regimes. It is also illustrated that increasing the number of BS antennas and the BS density provide varying degrees of benefits to counter the effects of beam alignment errors.

References

[1] X. Yu, J. Zhang, M. Haenggi and K. B. Letaief, "Coverage analysis for millimeter wave networks: The impact of directional antenna arrays," *IEEE J. Sel. Areas Commun.*, vol. 35, no. 7, pp. 1498–1512, July 2017.

[2] M. Cheng, J. Wang, Y. Wu, X. Xia, K. Wong and M. Lin, "Coverage analysis for millimeter wave cellular networks with imperfect beam alignment," *IEEE Trans. Veh. Technol.*, vol. 67, no. 9, pp. 8302–8314, Sep. 2018.

[3] A. Thornburg and R. W. Heath, "Ergodic capacity in mmWave ad hoc network with imperfect beam alignment," in *Proc. IEEE Military Commun. Conf. (MILCOM)*, Oct. 2015, pp. 1479–1484.

[4] N. Bahadori, N. Namvar, B. Kelleyy and A. Homaifar, "Device-to-device communications in millimeter wave band: impact of beam alignment error," 2019 Wireless Telecommunications Symposium (WTS), New York City, NY, USA, 2019, pp. 1–6.

[5] J. Wildman, P. H. J. Nardelli, M. Latva-aho and S. Weber, "On the joint impact of beamwidth and orientation error on throughput in directional wireless Poisson networks," *IEEE Trans. Wireless Commun.*, vol. 13, no. 12, pp. 7072–7085, Dec. 2014.

[6] S. Singh, M. N. Kulkarni, A. Ghosh and J. G. Andrews, "Tractable model for rate in self-backhauled millimeter wave cellular networks," *IEEE J. Sel. Areas Commun.*, vol. 33, no. 10, pp. 2196–2211, Oct. 2015.

[7] T. Bai and R. W. Heath, "Coverage and rate analysis for millimeter-wave cellular Networks," *IEEE Trans. Wireless Commun.*, vol. 14, no. 2, pp. 1100–1114, Feb. 2015.

[8] M. Shi, K. Yang, C. Xing and R. Fan, "Decoupled heterogeneous networks with millimeter wave small cells," *IEEE Trans. Wireless Commun.*, vol. 17, no. 9, pp. 5871–5884, Sep. 2018.

[9] A. Gaber and A. Omar, "Utilization of multiple-antenna multicarrier systems and NLOS mitigation for accurate wireless indoor positioning," *IEEE Trans. Wireless Commun.*, vol. 15, no. 10, pp. 6570–6584, Oct. 2016.

[10] M. Rebato, J. Park, P. Popovski, E. De Carvalho and M. Zorzi, "Stochastic geometric coverage analysis in mmWave cellular networks with realistic channel and antenna radiation models," *IEEE Trans. Commun.*, vol. 67, no. 5, pp. 3736–3752, May 2019.

[11] S. Balakrishnan, P. Wang, A. Bhuyan and Z. Sun, "Modeling and analysis of eavesdropping attack in 802.11ad mmWave wireless networks," *IEEE Access*, vol. 7, pp. 70355–70370, 2019.

[12] C. A. Balanis, *Antenna Theory: Analysis and Design, 4th ed.* Hoboken, NJ, USA: Wiley, 2016.

[13] D. A. Fittipaldi and M. Luise, "Cramér-Rao bound for DOA estimation with antenna arrays and UWB-OFDM signals for PAN applications," in *Proc. IEEE 19th Int. Symp. on Pers., Indoor and Mobile Radio Commun. (PIMRC)*, Sep. 2008, pp. 1-5.